Tectonophysics 760 (2019) 23–35

Contents lists available at ScienceDirect

Tectonophysics

journal homepage: www.elsevier.com/locate/tecto

Testing Early Cretaceous Africa–South America fits with new palaeomagnetic data from the Etendeka Magmatic Province (Namibia)

Trishya M. Owen-Smith[a,b,*], Morgan Ganerød[c], Douwe J.J. van Hinsbergen[d], Carmen Gaina[e], Lewis D. Ashwal[a], Trond H. Torsvik[a,c,e,f]

[a] School of Geosciences, University of the Witwatersrand, WITS, 2050 Johannesburg, South Africa
[b] Department of Geology, University of Johannesburg, 2006 Johannesburg, South Africa
[c] Geodynamics, Geological Survey of Norway, NO-7491 Trondheim, Norway
[d] Department of Earth Sciences, Utrecht University, Heidelberglaan 2, 3584 CS Utrecht, The Netherlands
[e] Centre for Earth Evolution and Dynamics (CEED), University of Oslo, 0315 Oslo, Norway
[f] Helmholtz Centre Potsdam, GFZ, Telegrafenberg, 14473 Potsdam, Germany

ARTICLE INFO

Keywords:
Paraná–Etendeka Large Igneous Province
South Atlantic Ocean opening
Palaeomagnetic reconstruction
Cretaceous palaeopole

ABSTRACT

We provide an independent test for the proposed pre-breakup fits between the South American and African continental margins based on new palaeomagnetic data. In the course of modelling the opening of the South Atlantic Ocean, several reconstructions have been proposed, which correspond to different estimates of the amount of pre-drift extension in the South American and African continental margins, and amounts of displacement along intracontinental accommodation zones. The Paraná–Etendeka Large Igneous Province erupted during a brief time interval between ~136 and ~131 Ma, just prior to opening of the South Atlantic, and has magmatic products on both the African (Etendeka lavas) and South American (Paraná lavas) plates. Here we provide new palaeomagnetic constraints on the Etendeka volcanic rocks. These yield a declination of $D \pm \Delta D_x = 314.4 \pm 7.0^\circ$ and inclination of $I \pm \Delta I_x = -42.7 \pm 8.3^\circ$ (Plat = 47.5, PLon = 88.9, K = 26.1, A95 = 6.3, n = 21). When our results are combined with another recently published dataset, we obtain an Etendeka palaeopole at 49.1° S, 87.6° E ($D \pm \Delta D_x = 315.9 \pm 3.8^\circ$, $I \pm \Delta I_x = -43.9 \pm 4.4^\circ$, K = 23.4, A95 = 3.5, n = 75). We compare three recent models for South Atlantic Ocean opening, discuss which of the models best fits the palaeomagnetic data, and present a revised reconstruction for West Gondwana during the Early Cretaceous.

1. Introduction

The opening of the South Atlantic Ocean was preceded, and likely triggered or aided, by the emplacement of the Paraná–Etendeka Large Igneous Province (LIP), which erupted at ~136–131 Ma and covered vast areas of Brazil, Uruguay, Paraguay and Argentina and parts of Namibia and Angola (Stewart et al., 1996; Kirstein et al., 2001; Dodd et al., 2015). The opening history of the South Atlantic is constrained by the geometric fits of the margins, marine magnetic anomalies, fracture zones, continental and oceanic structures and the timing of magmatic activity around the ocean basin (e.g., Torsvik et al., 2009; Moulin et al., 2010). Prior to and during Paraná–Etendeka magmatism, extension between South America and Africa was accommodated by intracontinental deformation, the amount and distribution of which is disputed, leading to a variety of full-fit reconstructions (e.g., Torsvik et al., 2009; Moulin et al., 2010; Solano et al., 2010; Pérez-Díaz and Eagles, 2014, and references therein).

Because the Paraná–Etendeka LIP covers continental crust of both the South American and African plates, the overlap between the palaeomagnetic poles derived from the South American Paraná and African Etendeka lavas, when corrected for South Atlantic opening, provides an independent reliability test for the various Early Cretaceous South America–Africa fits. There is an extensive palaeomagnetic dataset from the Paraná basalts in South America (Raposo and Ernesto, 1995; Ernesto et al., 1990, 1996, 1999; Tamrat and Ernesto, 1999; Alva-Valdivia et al., 2003; Mena et al., 2006; Solano et al., 2010; Goguitchaichvili et al., 2012), but until the recent study of Dodd et al. (2015), very few data existed for the Etendeka basalts. Dodd et al. (2015) studied the magnetostratigraphy and eruption timescales of the Etendeka basalts and provided a very welcome directional dataset for almost 100 lava sites in Namibia.

Here, we provide additional results for 29 sites from the Etendeka

* Corresponding author at: Department of Geology, University of Johannesburg, 2006 Johannesburg, South Africa.
E-mail address: trishyaos@uj.ac.za (T.M. Owen-Smith).

https://doi.org/10.1016/j.tecto.2017.11.010
Received 21 July 2017; Received in revised form 31 October 2017; Accepted 6 November 2017
Available online 08 November 2017
0040-1951/

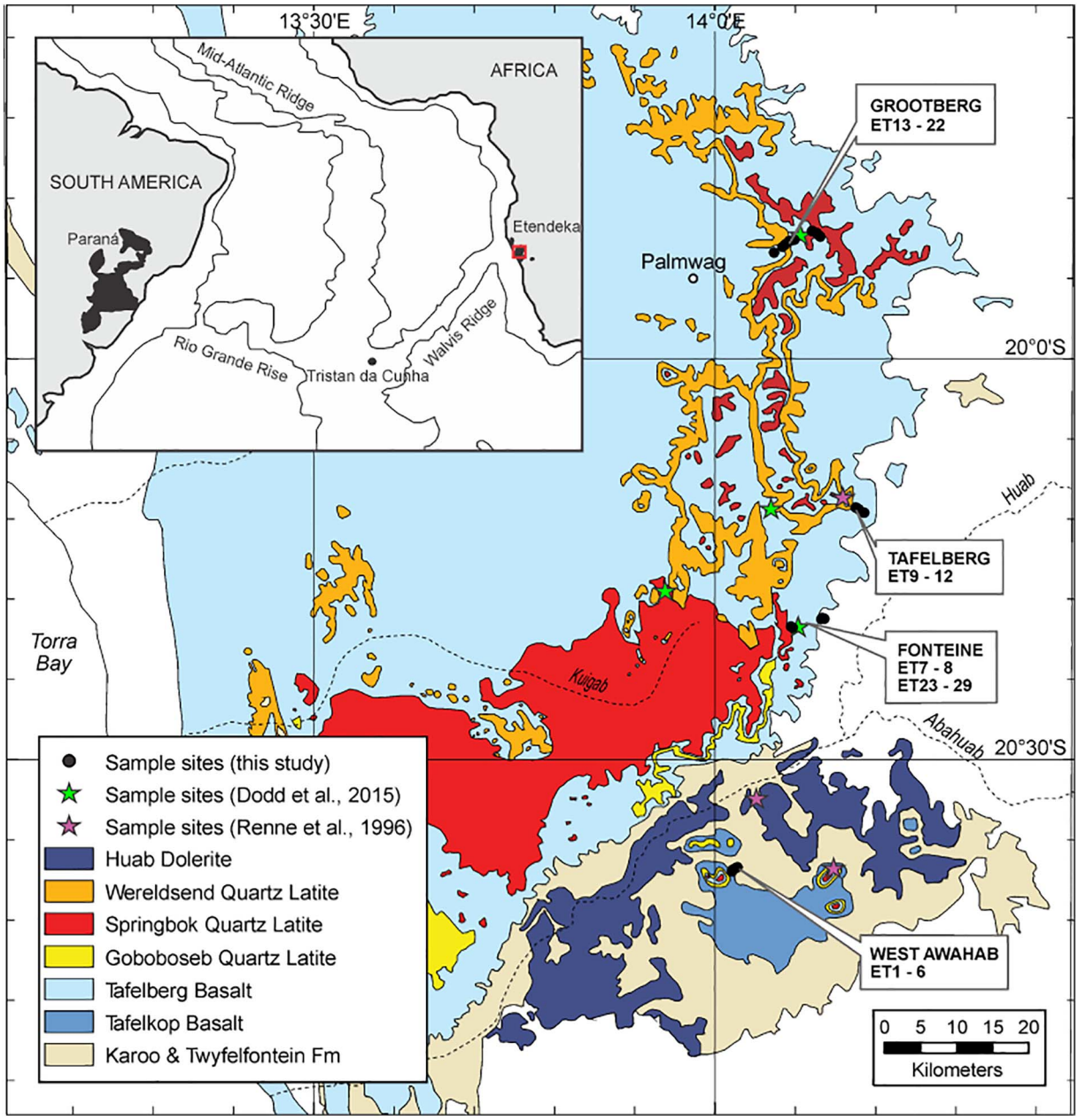

Fig. 1. Geological map of the main Etendeka lava field in Namibia (after Milner et al., 1992, and Miller, 2008) showing the locations of the four sections sampled in this study (Grootberg, Tafelberg, Fonteine and Awahab) and the numbers of the sites in each section (black circles). The stars indicate the approximate locations of sites sampled in the earlier studies of Renne et al. (1996) and Dodd et al. (2015). The inset shows the location of the study area (red box) with respect to the present-day continental configuration and outcrop of the Paraná and Etendeka volcanic rocks. (For interpretation of the references to colour in this figure legend, the reader is referred to the web version of this article.)

lavas, collected during a 2009 field campaign, and we re-examine the palaeomagnetic pole of the Etendeka basalts. We use our results to test the goodness of fit of three recently proposed models for continental separation during the opening of the South Atlantic Ocean (Torsvik et al., 2009; Moulin et al., 2010; Heine et al., 2013). In addition to the importance of the new dataset for South Atlantic reconstructions, it is vital that new palaeomagnetic poles from stable plate interiors are added to the palaeomagnetic database used to compute the Global Apparent Polar Wander Path (GAPWaP) that serves as the reference for palaeomagnetic studies worldwide. Our new data add a high-quality palaeomagnetic pole for the Early Cretaceous to that database.

2. Geological setting and previous work

The Etendeka Igneous Province, preserved in northern Namibia and southern coastal Angola (Fig. 1), is the African component of the Paraná–Etendeka LIP, and consists of an approximately 1000 m-thick bimodal volcanic succession and an intrusive suite (Miller, 2008, and references therein). The volcanic succession of tholeiitic basalts, basaltic andesites, latites and quartz latites has been subdivided into: 1) the Awahab Subgroup at the base, present in the south of the province and topped by a regional unconformity; 2) the Etaka Subgroup immediately above the unconformity in the central regions of the province; 3) the Khumib Formation in the north of the province; and 3) the Skeleton Coast Subgroup along the west coast (Miller, 2008). The volcanic units overlie, and in places interfinger with, aeolian sandstones of the Early Cretaceous Twyfelfontein Formation (Miller, 2008). Within the mafic and siliceous suites, distinct magma types have been identified from their compositions and regional distribution, and several of these have been correlated with equivalent magma types in the Paraná

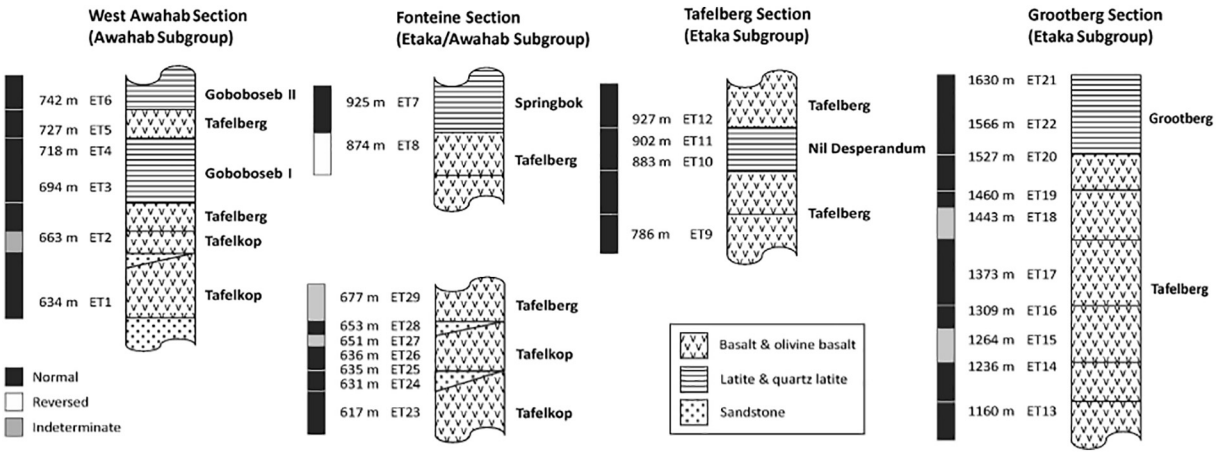

Fig. 2. Approximate stratigraphic positions, with their elevations relative to sea level, of samples taken in each of the 4 sampling sections in the main Etendeka lava field (see Fig. 1). Polarities for samples from each of the 29 sites (Table 1) are indicated. Not to scale.

Province (Alberti et al., 1992; Milner et al., 1992, 1995a; Peate et al., 1992; Peate, 1997; Marsh et al., 2001; Ewart et al., 2004a, 2004b).

Dating of the Etendeka volcanic rocks by $^{40}Ar/^{39}Ar$ and $^{87}Rb/^{86}Sr$ isochron methods has yielded ages between 133 and 128 Ma (assuming a Fish Canyon Tuff sanidine (FCTs) age of 27.84 Ma; Renne et al., 1996; Milner et al., 1995b; Stewart et al., 1996; Marzoli et al., 1999; Kirstein et al., 2001). A recent magnetostratigraphic investigation by Dodd et al. (2015) constrained the age range of the Etendeka volcanic rocks to ~136–131 Ma (premised on correlations with published $^{40}Ar/^{39}Ar$ ages calculated with a FCTs age of 28.205 Ma, from Renne et al., 2010), which we adopt as the age range for the volcanic succession. The intrusive suite (the Brandberg, Okenyenya, Okorusu, Erongo, Doros, Paresis, Otjohorongo, Etanenoberg, Spitzkoppe, Cape Cross and Messum Complexes, and various dykes and sills) shows a wider age range of 137 to 122 Ma (U–Pb zircon, $^{40}Ar/^{39}Ar$ and $^{87}Rb/^{86}Sr$ isochron ages; Manton and Siedner, 1967; Allsopp et al., 1984; McNeill, 1989; Milner et al., 1993, 1995b; Renne et al., 1996; Stewart et al., 1996; Pirajno et al., 2000; Schmitt et al., 2000; Verwoerd et al., 2000; Kirstein et al., 2001; Frindt et al., 2004; Wigand et al., 2004; Owen-Smith et al., 2017). The Paraná lavas and intrusive complexes cover a similar age range, from 138 to 126 Ma (U–Pb zircon and $^{40}Ar/^{39}Ar$ methods; Renne et al., 1992; Turner et al., 1994; Stewart et al., 1996; Kirstein et al., 2001; Lustrino et al., 2005; Thiede and Vasconcelos, 2010; Janasi et al., 2011; Pinto et al., 2011). However, the reliability of many of the earlier $^{40}Ar/^{39}Ar$ ages has been questioned (see discussions by Kirstein et al., 2001; Thiede and Vasconcelos, 2010; Janasi et al., 2011), and caution is advised when interpreting absolute ages in the Paraná–Etendeka LIP and other LIPs in general (Luttinen et al., 2015; Polteau et al., 2016; Wilkinson et al., 2016).

Numerous palaeomagnetic studies have been undertaken in the Paraná Province (e.g., Raposo and Ernesto, 1995; Ernesto et al., 1990, 1996, 1999; Tamrat and Ernesto, 1999; Alva-Valdivia et al., 2003; Mena et al., 2006; Solano et al., 2010; Goguitchaichvili et al., 2012), but until the recent study of Dodd et al. (2015), only one published study existed for the Etendeka lavas (Gidskehaug et al., 1975). The Etendeka volcanic succession is better exposed than the Paraná equivalents, and is generally flat-lying in the main lava field (Marsh et al., 2001). In the early study of Gidskehaug et al. (1975), 49 lavas sites were drilled in the main Etendeka volcanic field, of which only a grand mean pole was reported for 40 sites that predicted a palaeolatitude close to 24° S. Their K–Ar age estimate of 118 ± 4 Ma is considerably younger than ages provided by modern dating techniques and is likely unreliable, possibly representing an alteration date (Verati and Jourdan, 2014). Subsequently, Renne et al. (1996) provided magnetostratigraphic records for 39 sites in the Tafelkop, Awahab and Tafelberg sections (Awahab and Etaka Subgroups), but no directional data were published. The $^{40}Ar/^{39}Ar$ ages reported by Renne et al. (1996) are 132.1 ± 0.4 Ma to 131.9 ± 0.5 Ma for the Awahab section, and 132.3 ± 0.7 Ma for the base of the Tafelberg section (FCTs = 27.84 Ma), revealing no resolvable age differences between the base and top of the volcanic succession. These sections recorded only two magnetic reversals, during a period of known high geomagnetic reversal frequency (Gradstein et al., 1994; Gee and Kent, 2007) and were thus interpreted as representing rapid extrusion over a short time period (Renne et al., 1996). The recent study of Dodd et al. (2015) provided directional data for 99 lava sites, representing a nearly complete stratigraphic section in the southern Etendeka Province. Their study provided evidence for a more prolonged eruption timescale (> 4 m.y.) than that suggested by Renne et al. (1996). In our statistical analysis, we have included the data from Dodd et al. (2015).

3. Sampling

We sampled a total of 27 sites in basaltic and silicic lava flow units, as well as 2 sites in intercalated sandstones, from four sections in the main Etendeka lava field (Fig. 1): 1) the lower Awahab Subgroup west of Awahab Mountain, southeast of the main lava field (6 sites, West Awahab Section); 2) the Etaka and Awahab Subgroups at Fonteine in the main lava field (9 sites, Fonteine Section; similar to the section of the same name of Dodd et al., 2015); 3) the Etaka Subgroup at Tafelberg Mountain in the main lava field (4 sites, Tafelberg Section; close to the Tafelberg sampling site of Renne et al., 1996); and 4) the Etaka Subgroup at Grootberg Mountain in the northeastern part of the main lava field (10 sites, Grootberg Section; roughly equivalent to the Grootberg traverse of Dodd et al., 2015). The approximate stratigraphy of each sampled section is shown in Fig. 2. Each site has a minimum of 5 samples and in total, 228 samples were collected. Samples were drilled as 25 mm cores and were oriented by both magnetic and sun compass. All sampled lavas were approximately horizontal.

4. Methods

The magnetic mineralogy of the sampled rock types was investigated by means of reflected light microscopy and thermomagnetic experiments. Strong-field thermomagnetic experiments were performed on core samples using a horizontal Curie balance. Curie temperatures were determined graphically, from the intersection of the tangents of the curve segments on either side (Moskowitz, 1981). Room-temperature hysteresis loops, back-field curves and remanence coercivity (B_{cr}) were measured using a MicroMag 3900 Vibrating Sample Magnetometer (VSM) with field ranges of approximately 1–2 T.

Both stepwise thermal and alternating-field (AF) demagnetisation

was conducted at the palaeomagnetic laboratory of the Norwegian Geological Survey in Trondheim, to determine the components of natural remanent magnetisation (NRM) and their characteristics. Samples were thermally demagnetised in 10–16 steps between 150 and 590 °C, at intervals from 50 °C in low-temperature steps, down to 5 °C with increasing temperature. AF demagnetisation was performed in 20–25 steps of 1–10 mT, up to 100 mT. The remanent magnetisation of the specimens was measured using an AGICO JR6A dual-speed spinner magnetometer mounted within Helmholtz coils. The characteristic remanent magnetisation (ChRM) was determined by principle component analysis (PCA) and by using the LineFind algorithm (Kent et al., 1983), implemented in the Super-IAPD program (Torsvik et al., 2000). All site data are provided in the Supplementary information in a format that can be viewed in the 'NGU' format, using the paleomagnetism.org online analysis tool (Koymans et al., 2016). Fisher (1953) statistics were used to determine site means from the ChRM directions for the set of samples at each lava or sedimentary rock site, and to derive virtual geomagnetic poles (VGPs) from each of these site means, following the approach detailed in Deenen et al. (2011). Statistical analysis was performed on paleomagnetism.org (Koymans et al., 2016). The great circle principle of McFadden and McElhinny (1988) was used when samples did not show stable end points.

5. Results

5.1. Magnetic mineralogy

5.1.1. Optical microscopy

The principle opaque phase in all the volcanic rocks is titanomagnetite (Fig. 3), typically with sandwich-textured sectors of ilmenite oxy-exsolution (Fig. 3a). This indicates high-temperature (> 600 °C) deuteric oxidation during cooling, up to Class II of Haggerty (1991). In some cases, the titanomagnetite is altered to titanomaghaemite, evident as irregular patches and mottling in these grains (Fig. 3a, b). Secondary haematite is also present in the silicate phases, particularly along fractures in relict olivine.

In the basalts and olivine basalts, the opaque minerals make up 3 to 10 modal percent of the rocks. They range from 0.01 to 1 mm in size and are typically subhedral to anhedral, but may be skeletal (Fig. 3b). Titanomagnetite contents range from 5% to 8% in the quartz latites, commonly occurring as small subhedral rounded grains (0.02–0.1 mm), although long needles (up to 0.7 mm), are present in the Grootberg quartz latite sample, ET22 (Fig. 3c). The latites contain approximately 10% titanomagnetite, as characteristic comb-structured needles up to 0.1 mm long (Fig. 3d). In the intercalated sandstones, the opaque phase is minor rounded magnetite (~0.1 mm), typically constituting < 2% of the rock.

5.1.2. Thermomagnetic and hysteresis experiments

On the basis of the thermomagnetic results, we identify three groups of samples. In the first group, as in Fig. 4a, the dominant magnetic carrier phase is a Ti-poor titanomagnetite ($Fe_{3-x}Ti_xO_4$; $x \approx 0.1$, according to Dunlop and Özdemir, 1997) or pure magnetite (T_c = 550–580 °C). These samples show essentially reversible curves. The second group (e.g., Fig. 4b) shows a composite curve with a high Curie temperature feature (T_c = 570–650 °C), representative of low-temperature oxidation to titanomaghaemite, and a slight rise in magnetisation between 150 and 200 °C indicating the inversion of titanomaghaemite to haematite (Dunlop and Özdemir, 1997). These curves are irreversible. The third group (e.g., Fig. 4c) shows a single feature at T_c = 600–640 °C, indicating low-temperature maghaemitisation (Dunlop and Özdemir, 1997). All the cooling curves are lower than the

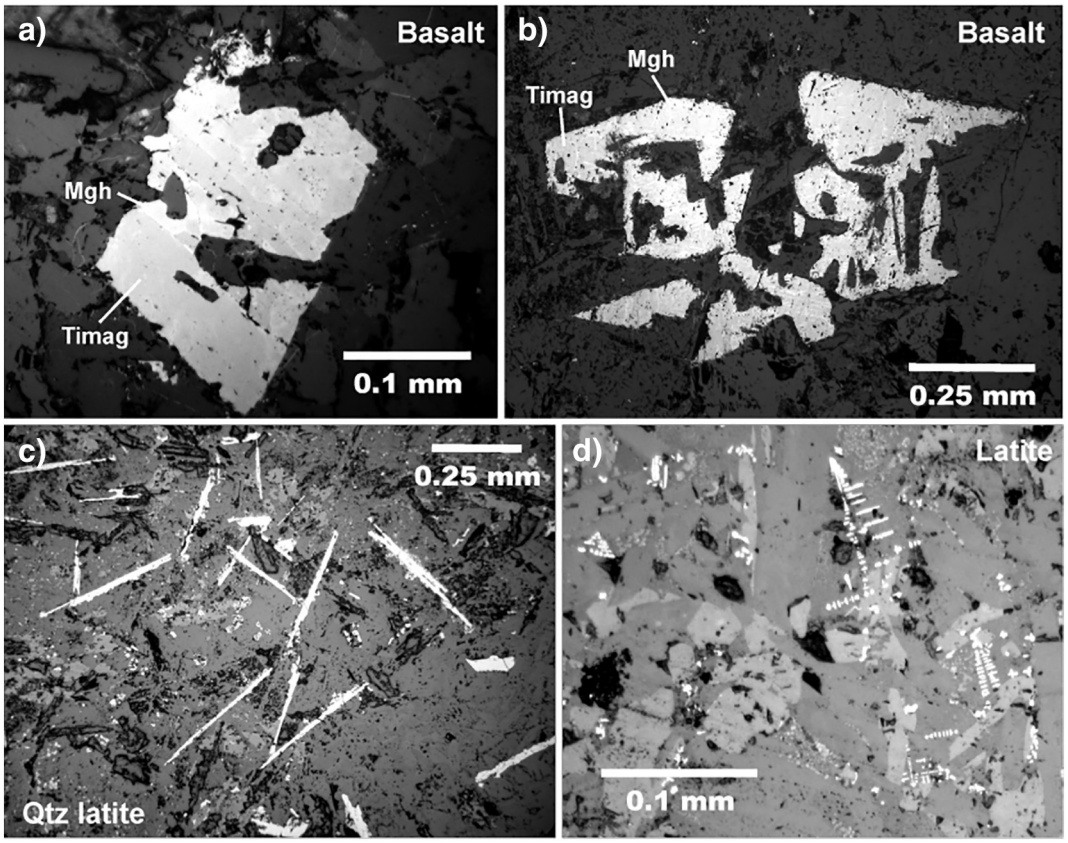

Fig. 3. Reflected light photomicrographs of opaque phases in the sampled Etendeka volcanic rocks. a) Subhedral equant titanomagnetite (Timag) with white maghaemite (Mgh) alteration in Tafelberg-type amygdaloidal basalt from the Etaka Subgroup (Site 16). b) Skeletal titanomagnetite with maghaemite alteration in Tafelkop basalt (Site 1). c) Needle-like phenocrysts of titanomagnetite in Grootberg quartz latite (Site 22). d) Comb-structured skeletal titanomagnetite phenocrysts in Nil Desperandum latite (Site 19).

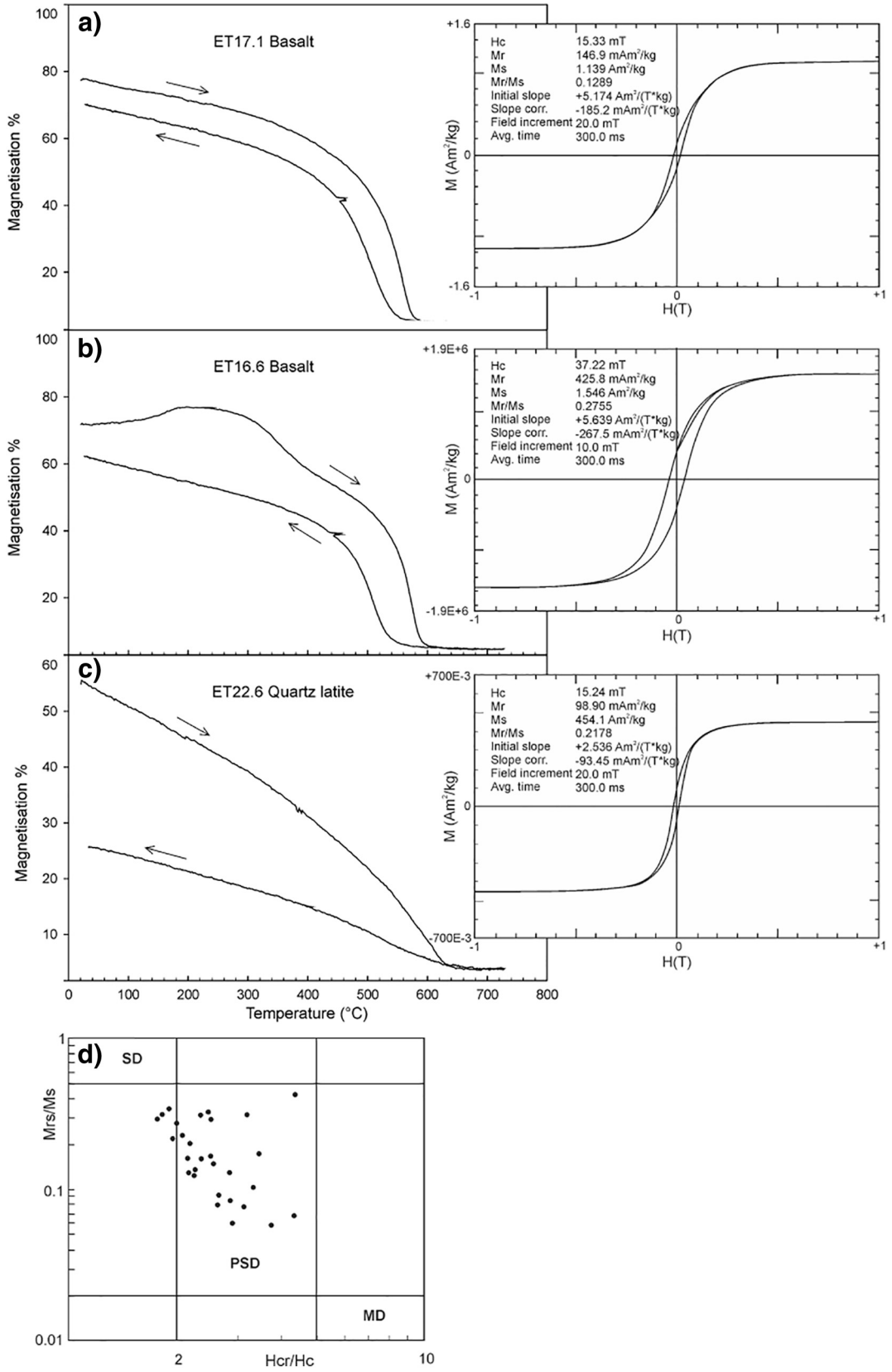

Fig. 4. Typical thermomagnetic curves for the Etendeka sample suite, and their corresponding hysteresis loops. a) Type 1, showing a Curie temperature of 580 °C, indicative of magnetite. b) Type 2, showing features of titanomagnetite weakly oxidised to titanomaghaemite, with a Curie temperature of 590 °C and an increase in magnetisation at ~200 °C due to inversion. c) Type 3. A high Curie temperature of 630 °C indicates titanomaghaemite. d) Hysteresis parameters M_{rs}/M_s versus H_{cr}/H_c (Day plot) for all samples, indicating that the carrier grains are predominantly pseudo-single domain grains. SD, single domain; PSD, pseudo-single domain; MD, multi-domain; M_{rs}, saturation remanence; M_s, saturation magnetisation; H_{cr}, remanent coercive force; H_c, ordinary coercive force.

Table 1
Palaeomagnetic sampling sites and results. D/I = declination/inclination of flow mean remanence directions; n = number of remanence directions successfully obtained; k and α_{95} are the Fisher, 1953 precision parameter and half angle of the cone of 95% confidence, respectively. NRM denotes moment intensities (mA) and Sus are the susceptibilities before heating. Q is the Königsberger ratio based on an ambient field strength of 51,673.4 nT (IGRF total field, Trondheim, Norway, 13.9.2010), which translates into 41.12 A/m. Site 8, marked with an asterisk, was interpreted by great circle analysis. Text in italics indicates data not used in the statistical analysis (reason given in Comments column).

Site	Lat (°S)	Long (°E)	Altitude (m)	*n*	D (°)	I (°)	*a*95 (°)	k	Plat (°)	Plong (°)	Comments	Sus (10^{-5} SI)	NRM	Q
1	20.63	14.04	634	5	332.2	− 39.9	7.6	102.3	− 64.12	94.36		13,152.68	827.22	1.54
2	*20.63*	*14.04*	*663*	–	–	–	–		–	–	*No good*	*18,226.042*	*4766.501*	*6.46*
3	20.63	14.03	694	6	337.5	− 43.5	3.0	499.8	− 68.78	86.82		30,723.475	2790.572	2.21
4	20.63	14.03	718	5	341.3	− 42.3	7.8	97.2	− 72.32	88.01		25,195.22	461.37	0.44
5	20.63	14.03	727	7	341.4	− 41.6	8.5	51.4	− 72.49	89.69		34,411.76	2999.63	3.61
6	*20.63*	*14.03*	*742*	*7*	*323.7*	*− 37.8*	*14.9*	*17.4*	*− 56.16*	*96.43*	*Too low k*	*51,179.09*	*460.23*	*0.23*
7	20.33	14.1	925	6	310.4	− 43.8	7.4	82.9	− 44.28	87.68		19,945.7	7293.83	8.9
8*	20.33	14.09	874	7	125.4	44.4	6.7	82.1	− 39.84	86.53		62,436.33	1093.04	0.46
9	20.19	14.19	786	7	314.8	− 38.0	4.0	228.7	− 47.87	94.32		19,513.2	661.82	0.83
10	20.19	14.18	883	5	302.7	− 53.2	6.5	139.5	− 37.83	76.53		758.37	136.96	4.39
11	20.18	14.18	902	7	320.4	− 37.6	4.8	159.1	− 53.02	95.65		5616.77	2186.82	9.48
12	20.18	14.17	927	7	322.7	− 43.6	6.3	86.6	− 55.33	88.28		25,101.96	738.92	0.74
13	19.87	14.07	1160	5	299.8	− 43.2	13.4	67.4	− 34.58	86.67		5363.36	2843	11.38
14	19.86	14.08	1236	7	288.7	− 53.2	4.4	189.2	− 26.07	75.33		6925.2	992.06	3.47
15	*19.86*	*14.09*	*1264*								*No good*	*11,096.23*	*15,840.64*	*34.51*
16	19.85	14.09	1309	7	300.9	− 49.5	8.4	52.6	− 36.04	80.41		11,842.73	2390.15	4.9
17	19.85	14.1	1373	6	341.3	− 50.7	7.3	85.2	− 69.6	65.83		14,731.29	2716.68	4.49
18a	*19.84*	*14.12*	*1443*	*6*	*314.9*	*− 45.1*	*7.8*	*74.7*	*− 48.22*	*85.96*	*Dual polarity*	*23,332.93*	*905.13*	*0.96*
18b	*19.84*	*14.12*	*1443*	*3*	*120.9*	*47.4*	*12.5*	*98.3*	*− 35.91*	*82.67*		*23,332.93*	*905.13*	*0.96*
19	19.84	14.12	1460	6	303.1	− 49.9	6.4	110.6	− 37.95	80.11		23,966.54	6606.47	6.98
20	19.84	14.13	1527	7	311.0	− 48.9	6.5	87.2	− 44.76	81.38		5448.08	1806.46	8.08
21	*19.85*	*14.13*	*1630*	*5*	*290.9*	*− 36.3*	*13.1*	*35.1*	*− 25.6*	*90.63*	*Too low k*	*11,609.57*	*547.62*	*1.15*
22	*19.84*	*14.13*	*1566*	*6*	*300.8*	*− 17.8*	*10.5*	*41.7*	*− 31.96*	*105.65*	*Too low k*	*10,068.54*	*11,680.8*	*28.62*
23	20.32	14.14	617	6	302.5	− 33.1	6.5	107.2	− 35.92	96.1		13,281.45	11,680.8	1.16
24	20.32	14.13	631	16	295.2	− 27.8	2.5	218.7	− 28.33	97.86	Sandstone	22.63	167.08	200.6
25	20.32	14.13	635	7	303.7	− 24.8	7.6	64.0	− 35.81	102.5	Sandstone; baked contact of 23	103.2	111.09	35.19
26	20.32	14.13	636	3	321.1	− 39.6	14.7	71.4	− 53.82	93.52		11,142.45	3023.99	5.82
27a	*20.32*	*14.13*	*651*	*2*	*299.5*	*− 21.2*	*17.8*	*199.0*	*− 31.3*	*103.41*	*Dual polarity*	*10,621.01*	*20,393.56*	*45.48*
27b	*20.32*	*14.13*	*651*	*3*	*168.7*	*35.8*	*17.4*	*51.3*	*− 83.69*	*280.83*				
28	20.32	14.13	653	11	304.5	− 24.9	4.6	99.5	− 36.58	102.7		102.21	84.06	20.44
29	*20.32*	*14.13*	*677*								*No good*	*16,567.01*	*23,543.71*	*35.9*

heating curves, indicating oxidation on heating during the experiments.

Room-temperature hysteresis loops were produced for one core sample from each site (Fig. 4). The results for all samples are consistent with the dominance of a ferromagnetic mineral with low coercivity. A Day plot (Fig. 4d) of the VSM results shows that the majority of the magnetic carrier grains are pseudo-single domain grains. From the microscopy, thermomagnetic experiments and hysteresis measurements, it is evident that the dominant carrier of NRM is Ti-poor titanomagnetite and that this NRM is in the form of thermoremanent magnetisation (TRM). The minor component of chemical remanent magnetisation (CRM) gained during low-temperature oxidation to titanomaghaemite should be in the same direction as the primary TRM, although the intensity of magnetisation is diminished. The calculated palaeomagnetic directions are thus likely not affected by this alteration (Dunlop and Özdemir, 1997). The fine-grained and commonly skeletal nature of the grains indicates fast cooling of the lavas and provides stable magnetisation for analysis.

5.2. Palaeomagnetic results

The results of the palaeomagnetic analysis are summarised in Table 1. The characteristic remanent magnetisation (ChRM) was successfully obtained for 175 samples. A few of these samples (~4%) show a single stable component of magnetisation (e.g., Fig. 5a, b); however, the majority of samples also show a secondary component that is removed in steps up to 425 °C or 15 mT (e.g., Fig. 5c, d). We interpret this component as a viscous remanent magnetisation (VRM) that in places may represent a present-day field overprint, but as in the case of Fig. 5d, also includes a reversed magnetisation overprint.

Site 24 consists of sandstone with a baked aureole along its contact (Site 25) with the lava of Site 23. The site average for the lava at Site 23 shares a Common True Mean Direction (CTMD) with the baked contact of Site 25, and can be classified as C, according to the method of McFadden and McElhinny (1990). Neither Site 23, nor the baked contact of Site 25, shares a CTMD with the sandstone of Site 24. This defines a positive baked contact test (McFadden and McElhinny, 1990), suggesting that the palaeomagnetic directions are primary and did not undergo regional remagnetisation. In addition, the 16 samples from the sandstone of Site 24 yield a k-value of 218.7 (where k is the best estimate of the Fisher precision parameter)—much higher than can be expected from palaeosecular variation alone (Deenen et al., 2011). Therefore, we interpret this site average as a spot reading of the palaeomagnetic field, equivalent to a lava site.

Of the 27 lava sites, three (2, 15, and 29) did not yield interpretable results. Two sites (18 and 27) yielded double polarities, which is not to be expected in lavas that cooled instantaneously in geological time. Both of these sites were sampled on steep slopes, and we speculate that there may have been some displacement of material. These sites were omitted from further statistical analysis.

Lastly, since the scatter of palaeomagnetic directions within one lava site should be minimal, and related to measuring errors, we applied the standard cut-off by omitting sites with $k < 50$ (e.g., Biggin et al., 2008). This eliminated sites 6, 21, and 22. The remaining 19 lava sites and single sandstone site are interpreted to provide a reliable recording of the palaeomagnetic field (Fig. 6a) during eruption of the Etendeka lavas. Only one of these sites (Site 8) yielded reversed polarity, which is insufficient for a meaningful reversal test.

Thus, the useable data record consistent normal polarities through the Grootberg, Tafelberg and West Awahab sections (Fig. 1), whereas the Fonteine section records normal polarities with an interval of reverse polarity prior to eruption of the Springbok quartz latites. The magnetostratigraphy for the Grootberg, Tafelberg and Fonteine sections is consistent with that recorded by Renne et al. (1996) and Dodd et al. (2015) in equivalent sections. However, we note that the reverse

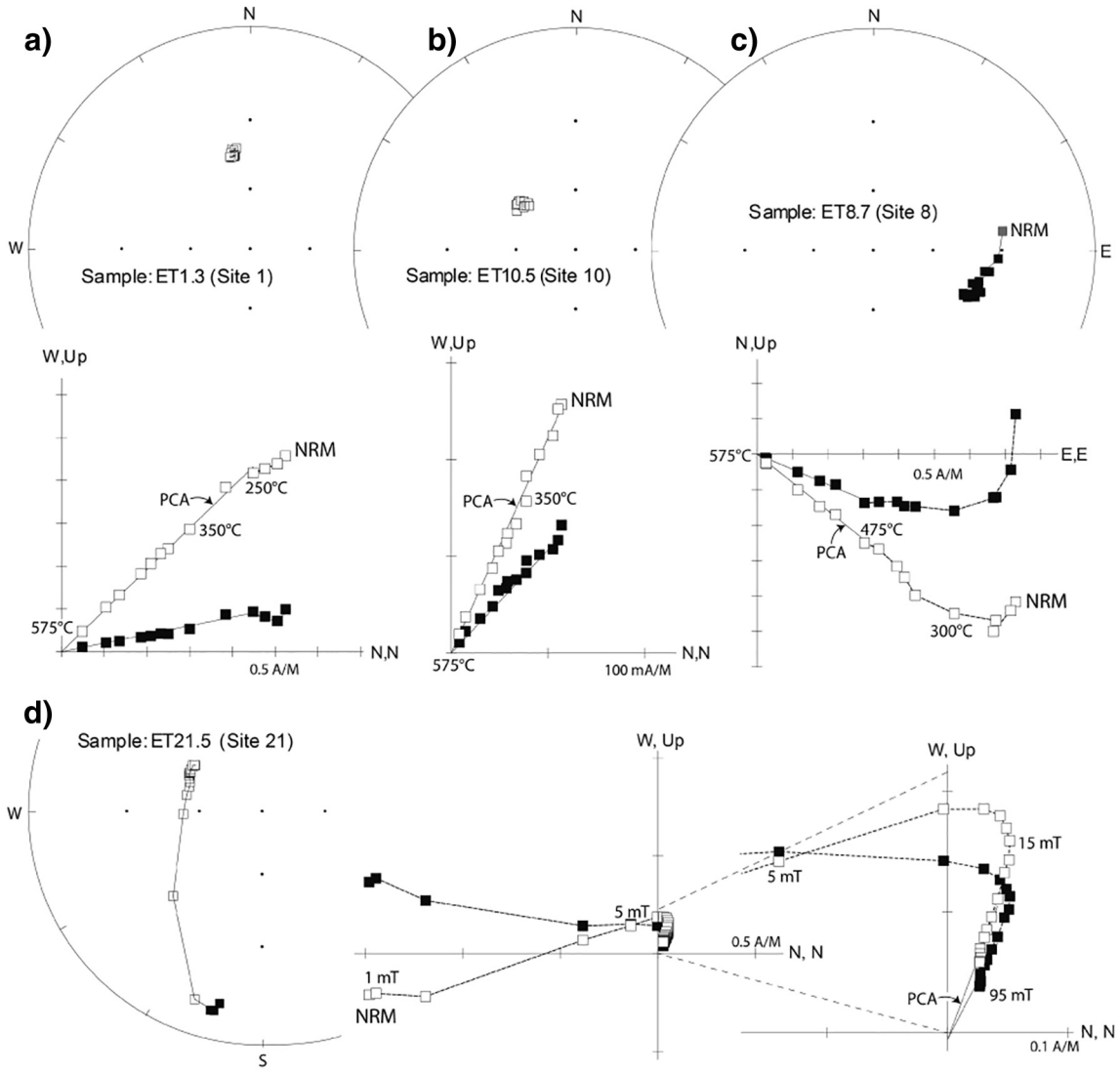

Fig. 5. Examples of stepwise thermal and alternating-field demagnetisation data represented as both orthogonal vector (Zijderveld) and stereographic plots. In the orthogonal plots, open squares represent projections onto the horizontal plane; closed squares represent projections onto the vertical plane. In the stereoplots, open circles represent normal polarities and closed circles represent reversed polarities. a) and b) are examples of almost simple component normal-polarity NRMs (natural remanent magnetisations) with a linear decay towards the origin from 250 °C and 150 °C, respectively. c) Example of a reverse direction, where the high temperature component is identified above 475 °C. d) A more complex alternating field demagnetisation pattern with a secondary low-intensity component overprinting the primary component of magnetisation, evident in the zoomed-in view. The corresponding stereoplot is also shown at left. PCA, principal component analysis.

polarities for the Grootberg quartz latites documented by Renne et al. (1996) at Awahab Mountain were not observed in our West Awahab traverse approximately 15 km to the west.

The combined mean direction of our sites was calculated by converting the reversed polarity of Site 8 to normal polarity. It was not necessary to remove any sites using a constant 45° or Vandamme (1994) variable cut-off angle. We determine a mean direction (Table 2) at reference location 20° S, 14.1° E of D ± ΔD_x = 314.4 ± 7 and I ± ΔI_x = − 42.7 ± 8.3 (n = 21). From this we calculate a palaeomagnetic pole for our study at 47.5° S and 88.9° E (K = 26.1; A95 = 6.3). This A95 value falls within the confidence envelope of Deenen et al. (2011), with $A95_{min}$ = 3.6 and $A95_{max}$ = 12.0, indicating that the data scatter can be explained by simple palaeosecular variation. The resulting pole (Fig. 6b) overlaps within error with the GAPWaP of Torsvik et al. (2012).

To increase our statistical power, we combined our data with those of Dodd et al. (2015). All data are provided in the Supplementary information. These authors reported consistent results from 70 sites, from which we removed 16 sites because they contained k-values smaller than 50. Dodd et al. (2015) divided their dataset into two parts, separated by an unconformity. The datasets from above and below the unconformity, as well as our new dataset, provide poles that are statistically indistinguishable and share a CTMD at the B level (McFadden and McElhinny, 1990). All data combined also provide a positive reversal test at the B level (McFadden and McElhinny, 1990). Thus, we calculate a palaeomagnetic pole position at 49.1° S and 87.6° E (n = 75; K = 23.4; A95 = 3.5; Table 2). This A95 value falls within the $A95_{min, max}$ envelope (2.1, 5.4) of Deenen et al. (2011), suggesting that the scatter can be explained by palaeosecular variation. No data points were removed by the 45° cutoff, and we use this pole in the following discussion.

Our pole (Fig. 6b; Table 2) is identical to a pole calculated by Gidskehaug et al. (1975), based on 49 lava sites, and shares a CTMD at the A level (McFadden and McElhinny, 1990). Gidskehaug et al. (1975), however, do not provide any information on site statistics, and we do not combine our data with theirs. Nevertheless, the similarity in the result demonstrates the reproducibility of the data and strengthens our confidence that the Etendeka palaeomagnetic pole is reliable.

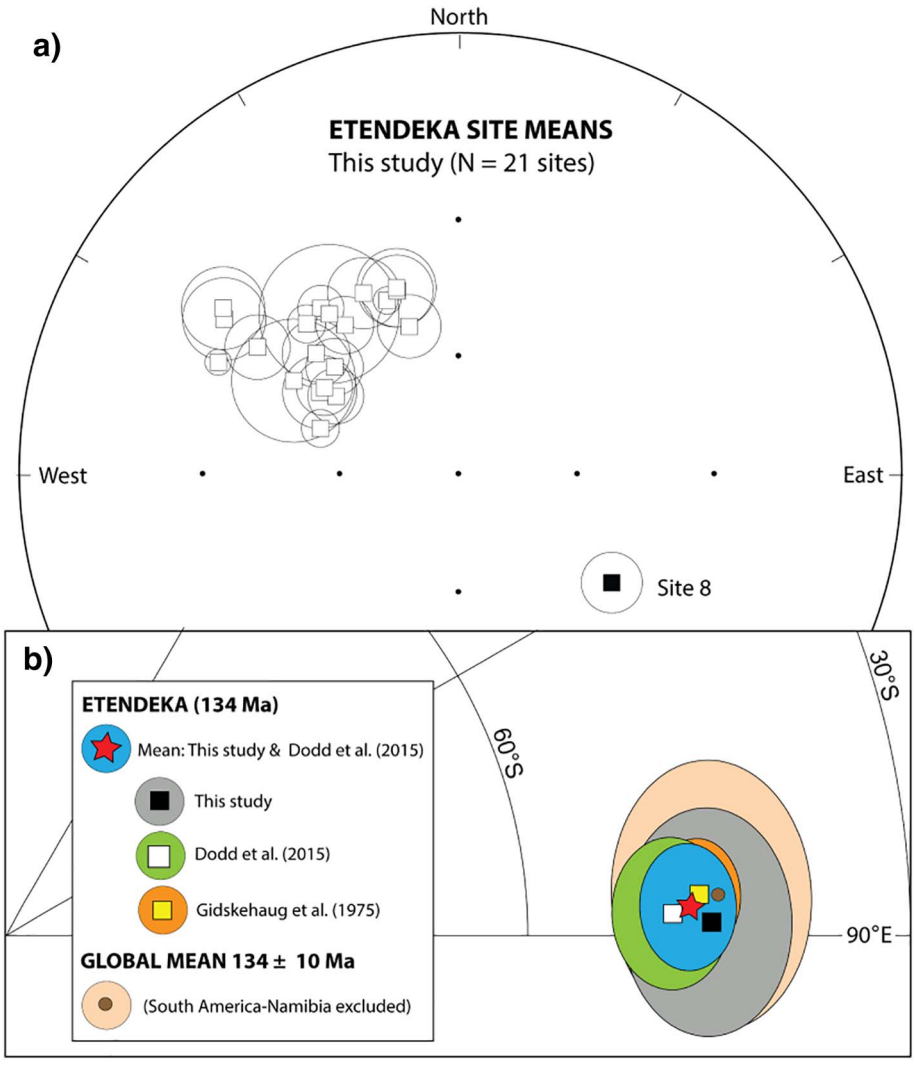

Fig. 6. a) Etendeka site mean directions and α_{95} ellipses for our new data (Table 1). b) The Etendeka palaeopole calculated from this study (black square, with dark grey A95 confidence oval), is shown in comparison with the mean pole from Dodd et al. (2015; white square), the early study of Gidskehaug et al. (1975; yellow square), and the global mean pole at 134 Ma (brown circle), excluding all Paraná–Etendeka poles (Torsvik et al., 2012). The red star with blue confidence oval is the grand mean palaeopole for the Etendeka Province based on this study and that of Dodd et al. (2015). (For interpretation of the references to colour in this figure legend, the reader is referred to the web version of this article.)

6. Testing Africa–South America fits

We now use our palaeomagnetic pole for the Etendeka lavas in combination with previous palaeomagnetic poles from the Paraná basalts in South America that are derived from similarly large datasets (e.g., Ernesto et al., 1990, 1999; Solano et al., 2010) to evaluate some recently published Africa–South America fits prior to the opening of the South Atlantic Ocean (Torsvik et al., 2009; Moulin et al., 2010; Heine et al., 2013). These fits are guided by the interpretation of marine magnetic anomalies, and estimates for the amount and distribution of pre-drift extension. The latter step, in particular, is associated with uncertainty, and different approaches have been attempted (see e.g., Pérez-Díaz and Eagles, 2014, for an overview).

Palaeomagnetic data from the time-equivalent Etendeka and Paraná volcanic rocks can provide an independent constraint on this fit: a successful fit should overlap the poles from the Etendeka and Paraná volcanic rocks when the Paraná poles are rotated into African coordinates using the total reconstruction pole of each fit. We evaluate fits (Fig. 7) proposed in the last decade by Torsvik et al. (2009), Moulin et al. (2010) and Heine et al. (2013).

There are much more palaeomagnetic data reported from the Paraná lavas and contemporaneous or younger dykes than from the Etendeka Magmatic Province. Here we use only the most reliable data from the Paraná lavas, but in order to test the model that includes significant displacement along the Paraná–Etendeka Fracture Zone (PEFZ; Torsvik et al., 2009), we recalculated some of the data because

Table 2
Palaeomagnetic poles calculated for the Etendeka lavas. Lat = latitude of the reference location; Lon = longitude of the reference location; *n* = number of lava sites used in the calculation; D = declination, ΔDx = error in declination sensu Butler (1992); I = inclination; ΔIx = error in inclination sensu Butler (1992); Plat = palaeolatitude of the virtual geomagnetic pole; Plon = palaeolongitude of the virtual geomagnetic pole; K = Fisher (1953) precision parameter of the pole; A95 = 95% cone of confidence around the pole; $A95_{min, max}$ = the minimum and maximum A95 for which the given *n* can be straightforwardly explained by palaeosecular variation of the palaeomagnetic field, sensu Deenen et al. (2011). Bold text highlights the Etendeka palaeopole calculated from the combined data from this study and that of Dodd et al. (2015), which we use to evaluate various Africa–South America fits in Section 6.

Study	Lat (°S)	Long (°E)	n	D (°)	ΔDx	I (°)	ΔIx	Plat (°S)	Plong (°E)	K	A95	A95min	A95max
This study	20.0	14.1	21	314.4	7	− 42.7	8.3	47.5	88.9	26.1	6.3	3.6	12.0
Dodd et al., 2015	20.0	14.1	54	316.6	4.7	− 44.4	5.3	50.3	88.1	22.3	4.2	2.4	6.6
Combined Etendeka pole	**20.0**	**14.1**	**75**	**315.9**	**3.8**	**− 43.9**	**4.4**	**49.1**	**87.6**	**23.4**	**3.5**	**2.1**	**5.4**
Gidskehaug et al., 1975	20.0	14.1	40					48.3	86.6	53.3	3.1		

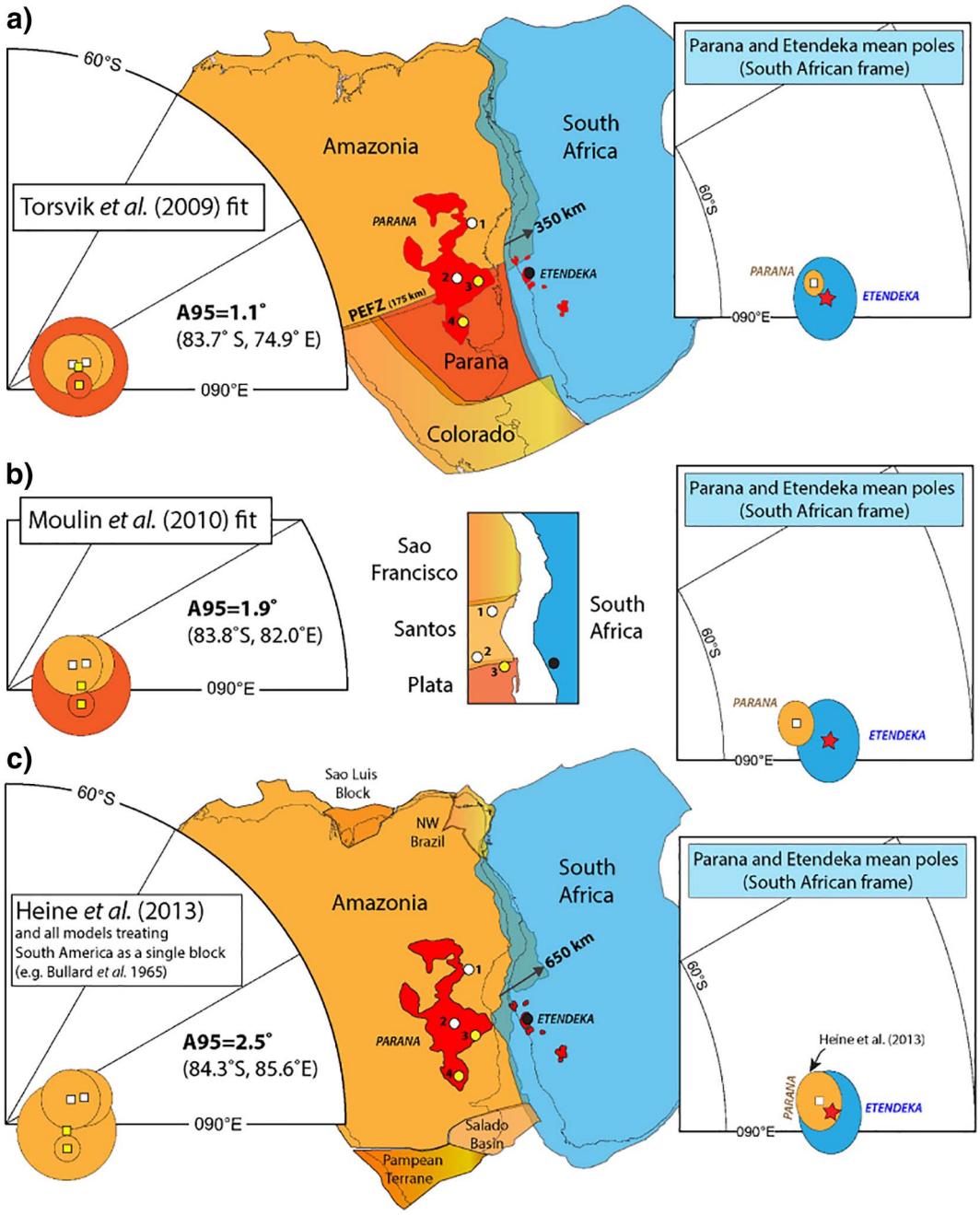

Fig. 7. Comparison of palaeopoles from South America and the Etendeka. a) The left hand plot shows four poles (Table 3) for the Paraná Province, fitted using the plate circuits of Torsvik et al. (2009): two from south (dark orange ovals) of the Paraná–Etendeka Fracture Zone (PEFZ), and two from north of this (part of the Amazonia block). The right hand plot shows the mean Paraná pole (orange) rotated to Africa at 134 Ma, relative to the new Etendeka pole (blue) from this study. b) The same plots as in (a), but calculated using the intraplate model of Moulin et al. (2010). c) The equivalent plots, fitted with the plate model of Heine et al. (2013). (For interpretation of the references to colour in this figure legend, the reader is referred to the web version of this article.)

the reported mean poles include sites from both sides of the PEFZ. Table 3 lists four poles from the Paraná volcanic succession. Two of these come from north of the PEFZ (named the Amazonia block in Torsvik et al., 2009), and two from the south. Along this fracture zone (also referred to as the Parana-Chacos Basin deformation zone by Unternehr et al., 1988, and Nürnberg and Müller, 1991), the southern part of South America (the Paraná block of Torsvik et al., 2009) moved relative to the northern part (the Amazonia block) during the opening of the South Atlantic Ocean. The Paraná block fits directly against the Etendeka margin of the South African domain of the African plate. The Amazonia block, however, is the conjugate margin to the NW Africa block, which underwent Cretaceous motion along intracontinental faults within Africa. All the various models tested require restoring the NW Africa–South Africa relative motion (as detailed in Torsvik et al., 2009), which is taken into account when conducting the palaeomagnetic test on the South Atlantic fits.

The reconstruction of Torsvik et al. (2009) entails the largest motion along the PEFZ of all the models tested (175 km of right-lateral transtensional displacement in the Early Cretaceous), and yields a near-perfect match with the three Paraná poles used in the test, with an A95 of 1.1° (Fig. 7a). Moulin et al. (2010) applied a different intraplate deformation model, and separated the Paraná block of Torsvik et al. (2009) into two parts, the Plata and Santos fragments. However, their PEFZ has a smaller total displacement than in Torsvik et al. (2009). The

Table 3
Palaeomagnetic mean poles from the Paraná lavas (recalculated, see text), which are of the same age as the Etendeka lavas (Table 2). *n* = number of sites/sections/lava flows; Plat = palaeolatitude of the virtual geomagnetic pole; Plong = palaeolongitude of the virtual geomagnetic pole; A95 = 95% cone of confidence around the pole; Plate Id. = -plate identification number in GPlates/Plates. Note that the combined Paraná pole (bold text) is given in both Amazonia and South African frames using the plate circuits of Torsvik et al. (2009).

Original study	Block (Plate Id.)	n	A95	Plat (°S)	Plong (°E)
Ernesto et al. (1990, 1999)	Amazonia (201)	92 (sites)	2.5	83	71.4
Ernesto et al. (1990)	Amazonia (201)	6 (sections) (96 flows)	2.5	84.1	69.2
Ernesto et al. (1990)	Parana (202)	10 (sections) (173 flows)	1,1	84.4	111.6
Solano et al. (2010)	Parana (202)	29 (lava flows)	4.2	84.8	95.8
Combined Paraná pole	**Amazonia (201)**	**4 (studies)**	**1.1**	**83.7**	**74.9**
Combined Paraná pole	**South Africa (701)**	**4 (studies)**	**1.1**	**50.4**	**85.5**

rotation parameters in Moulin et al. (2010) yield a larger A95 of 1.9°, and hence a somewhat poorer fit (Fig. 7b). Heine et al. (2013) did not invoke any motion along the PEFZ in their model. This scenario requires very high pre-drift extension values of as much as 650 km between Amazonia and Africa (compared to 350 km in Torsvik et al., 2009), and yields the poorest fit with the palaeomagnetic data from the Paraná and Etendeka successions, with an A95 of 2.5° (Fig. 7c).

The analysis of the three Paraná poles favours the fit of Torsvik et al. (2009), where the PEFZ was modeled as a transtensional zone with a large offset (175 km). The PEFZ is important, not only to reduce the extended continental margin overlap on the Brazilian (Santos) margin to realistic numbers, but extension along this fault would made it easier, and offer a preferred location, for plume-related volcanism to occur (by upside-down drainage). This would explain the large extent of Paraná volcanism compared to the Etendeka on the conjugate Namibian margin. There is, however, no consensus from either the surface geology or from geophysical data as to the exact location of intraplate deformation in the South American continent. Nevertheless, we note that the PEFZ is recognised in the GOCE (Gravity field and Ocean Circulation Explorer) free-air residual gravity field (Braitenberg, 2015) and in crustal and lithospheric thickness maps (e.g., Assumpção et al., 2013; Chulick et al., 2013), which to some extent reflect the Ediacaran to Early Cambrian juxtaposition of different Precambrian cratonic blocks (Paranapanema and Rio de la Plata cratons) during Gondwana formation (Fig. 9).

Closing the South Atlantic Ocean (rotating the mean Paraná pole to the South African frame) shows that the mean Paraná and Etendeka poles are in excellent agreement (Fig. 7a, right-hand diagram). The Moulin et al. (2010) closure model gives a poorer fit (Fig. 7b, right-hand diagram), but the two mean poles overlap at the 95% confidence level. The fit between Amazonia and Africa in the Heine et al. (2013) model is quite similar to that of Torsvik et al. (2009); thus, the reconstructed Paraná and Etendeka poles (Fig. 7c) are similar to that of Torsvik et al. (2009), except for the larger A95 for the mean Paraná pole because of no movement along the PEFZ.

7. Palaeogeographic implications

By combining our new palaeomagnetic results with an interpretation of early sea-floor spreading (Table 4), we can present a coherent model for the pre-breakup and early history of the South Atlantic opening between South America and Africa in the region of the Paraná–Etendeka LIP.

Table 4
South America relative to South Africa finite rotations for breakup time and early opening of the South Atlantic Ocean (after Gaina et al., 2013).

Age (Ma)	Chron	Rotation		
		Latitude	Longitude	Angle
112		52.4	− 35	51.3
121	M1ny	51.4	− 35	52.6
125.7	M4ny	50.6	− 33.8	54.2
127.79	M8ny	50.1	− 33.6	54.98
128.93	M10ny	49	− 33.3	55.66
130.00 (breakup)		48.4	− 33.3	56.18
134.00[a] (pre-breakup)		50	− 32.5	55.1

[a] Torsvik et al. (2009).

The opening of the Central Atlantic led to the complete separation of North and South Pangaea, with the result that much of the Palaeozoic Gondwanan continent (Torsvik and Cocks, 2017) regained its independence for a short time before Gondwana split into West and East Gondwana at ~170 Ma (Gaina et al., 2013) through opening of the West Somali Basin between East Africa and Madagascar–India. Gondwana steadily fragmented as the Cretaceous progressed, and the precursor to West Gondwana fragmentation is represented by the intrusion and eruption of the Paraná–Etendeka LIP at around 136–131 Ma (Fig. 9a).

The exact timing of the South Atlantic Ocean opening is a topic of much debate, as the geophysical signature of the crust formed after continental breakup is either masked by volcanic material or displays a complex pattern, untypical for oceanic crust (e.g., Moulin et al., 2010). Sea-floor spreading marine magnetic anomalies in the southern South Atlantic (Fig. 8) indicate an Early Cretaceous age for oceanic crust dated as chron M10, or ~134–129 Ma, depending on the timescale used (Gaina et al., 2013; Koopmann et al., 2014; Collier et al., 2017). We have dated the isochrons following the Gee and Kent (2007) timescale, where M10n is from 128.93 to 129.25 Ma.

The palaeomagnetic data place the products of Paraná–Etendeka magmatism at latitudes between 15 and 30° S (Paraná) and 26–32° S (Etendeka) at the time of eruption. Paraná–Etendeka and contemporaneous kimberlite activity (Fig. 9a) in West Gondwana (South Africa, Namibia, northwest Africa) was likely sourced by deep plumes from the western margin of the TUZO large low shear-wave velocity province (Torsvik and Cocks, 2017). Our data suggest that after the opening of the South Atlantic Ocean and the fragmentation of West Gondwana, South America has essentially moved only westward (~30°) with hardly any latitude change.

Our reconstruction at 134 Ma (Fig. 9a) shows the South American and African plates in their pre-breakup position, shortly before or just at the time of LIP eruption. A model for oceanic crust age around the African continent (Gaina et al., 2013) postulates that the oldest magnetic anomaly in the oceanic domain west of the Etendeka is c. 127.8 Ma (M8 by the Gee and Kent, 2007, timescale). A more recent study (Collier et al., 2017) argues that the first linear magnetic anomaly south of the Walvis Ridge is M3, but at the same time brings evidence that sea-floor spreading (possibly sub-aerial) may have commenced long before, but its magnetic signature was altered by the emplacement of volcanic material as seaward-dipping reflectors. Given the closeness in timing of Paraná–Etendeka flood volcanism and the generation of new oceanic crust, it is likely that the emplacement of this LIP assisted the subsequent continental breakup, as is the case for many other LIPs worldwide (e.g., Buiter and Torsvik, 2014).

Moreover, vigorous magmatic activity continued after continental breakup and early sea-floor spreading, as shown by the existence of seaward-dipping reflectors (SDRs) mapped on both sides of the South Atlantic Ocean (Fig. 9b, c; e.g., Koopmann et al., 2014, and references therein). According to interpreted marine magnetic anomalies and SDR

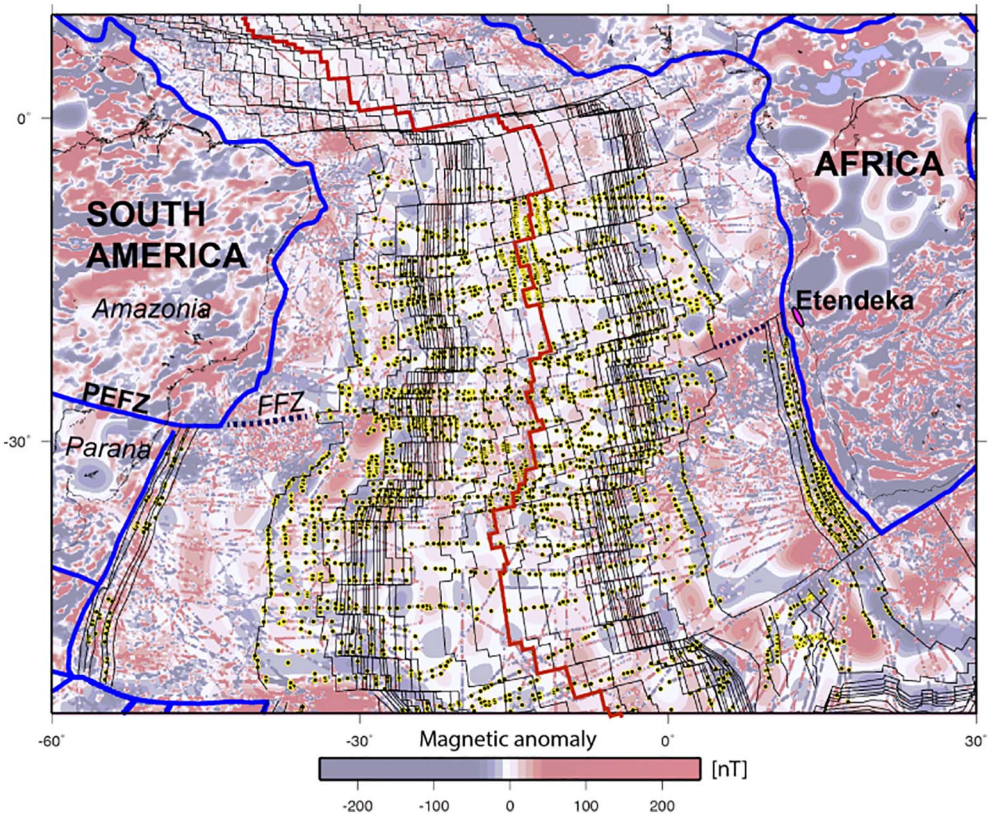

Fig. 8. Magnetic anomaly grid (WDMAM; Maus et al., 2007) of the South Atlantic region. Yellow circles show the location of identified magnetic anomaly picks (from the Seton et al., 2014, global compilation) and thin black lines are oceanic lithospheric isochrons (Gaina et al., 2013). The present-day mid-ocean ridge location is indicated by the thick red line. The continent–ocean boundaries (COBs) are shown as thick blue lines (African COB from Gaina et al., 2013; South American COB from Torsvik et al., 2009). These COBs are similar to those of Heine et al. (2013), except that they show a much more outboard COB on the Brazilian (Santos Basin) margin. FFZ, Florianopolis Fracture Zone; PEFZ, Paraná-Etendeka Fracture Zone. (For interpretation of the references to colour in this figure legend, the reader is referred to the web version of this article.)

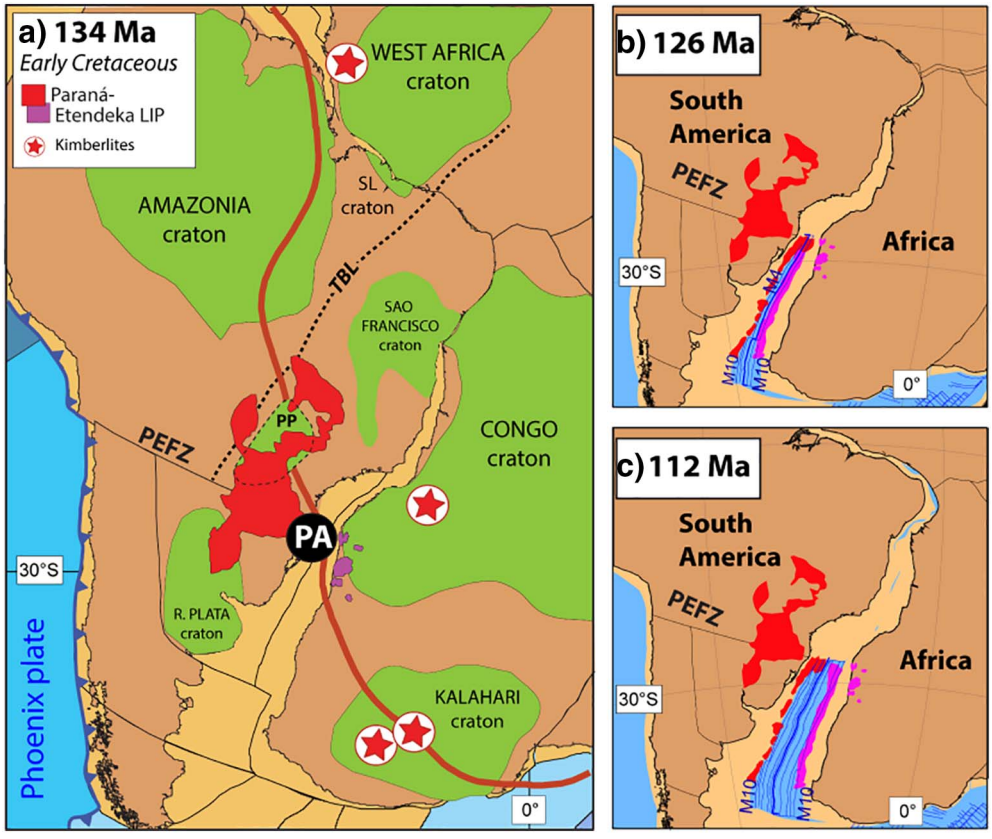

Fig. 9. Early Cretaceous palaeomagnetic reconstructions. a) Reconstruction at 134 Ma where the TUZO plume generation zone (PGZ, thick red line) is counter-rotated to account for true polar wander (Torsvik et al., 2012), so that the reconstructed Paraná–Etendeka (PA) LIP and kimberlites (within ± 5 Ma) from the Kalahari, Congo and West Africa cratons can be related to the deep mantle. Archaean and Palaeoproterozoic cratons (shaded green) in South America and Africa are after Casquet et al. (2012) and Dirks et al. (2009), respectively. PEFZ, Paraná-Etendeka Fracture Zone; PP, Paranapanema craton; SL, Sao Luis craton; TBL, Trans-Brasiliano Lineament. b) and c) Reconstructions at 126 Ma and 112 Ma, respectively. Thin blue lines are isochrons identified from magnetic data (Fig. 8). M10 and M4 indicate sea-floor spreading isochrons (see Table 4 for their ages). Seaward-dipping reflectors on the South American and African margins are modified from Koopmann et al. (2014). (For interpretation of the references to colour in this figure legend, the reader is referred to the web version of this article.)

extents, the Paraná–Etendeka magmatic activity may have stopped just prior to 112 Ma (Fig. 9c), followed by sea-floor spreading propagation north of the Florianopolis Fracture Zone (Fig. 8).

8. Conclusions

This study provides new palaeomagnetic data for the Early Cretaceous Etendeka volcanic succession. By combining our data with previous results from the Paraná–Etendeka LIP, we have generated a new Early Cretaceous pole for Africa, which overlaps with the GAPWaP of Torsvik et al. (2012) in African coordinates, and provides new constraints for future GAPWaP renditions. In addition, we have used this new mean pole to evaluate three recent models of South America–Africa fits prior to the opening of the South Atlantic Ocean. The palaeomagnetic results presented in this paper best fit the reconstruction of Torsvik et al. (2009). These results place the products of Paraná–Etendeka flood volcanism at latitudes of 15–32° S, and over a deep mantle plume generation zone, at the time of eruption at ~136–131 Ma, which was shortly before the initiation of sea-floor spreading in this region (~129–125 Ma).

Acknowledgements

We thank Statoil (the African Plate Project) for financial support for fieldwork in Namibia. CG and THT acknowledge the Research Council of Norway through its Centres of Excellence funding scheme, project number 223272. DJJvH acknowledges ERC Starting Grant 306810 (SINK) and NWO Vidi grant 864.11.004. We thank Cynthia Labails, Susan Webb, Roy Miller, Sergey Medvedev, Stephanie Werner and Tom Jordan for their help in the field. We also acknowledge the constructive comments of Lucia Pérez-Díaz and an anonymous reviewer.

Appendix A. Supplementary data

The Etendeka.pmag file contains all palaeomagnetic directions from this study, Dodd et al. (2015), and Gidskehaug et al. (1975) and can be uploaded and viewed at www.paleomagnetism.org (Koymans et al., 2016). Supplementary data associated with this article can be found in the online version, at https://doi.org/10.1016/j.tecto.2017.11.010.

References

Alberti, A., Piccirillo, E.M., Bellieni, G., Civetta, L., Comin-Chiaramonti, P., Morais, E.A., 1992. Mesozoic acid volcanics from southern Angola: petrology, Sr–Nd isotope characteristics and correlation with the acid stratoid volcanic suites of the Paraná basin (south-eastern Brazil). Eur. J. Mineral. 4, 597–604.

Allsopp, H.L., Bristow, J.W., Logan, C.T., Eales, H.V., Erlank, A.J., 1984. Rb–Sr geochronology of three Karoo-related intrusive complexes. Special Publications of the Geological Society of South Africa 13, 281–287.

Alva-Valdivia, L.M., Goguitchaichvili, A., Urrutia-Fucugauchi, J., Riisager, J., Riisager, P., Ferreira Lopes, O., 2003. Paleomagnetic poles and paleosecular variation of basalts from Paraná Magmatic Province, Brazil: geomagnetic and geodynamic implications. Phys. Earth Planet. Inter. 138, 183–196. http://dx.doi.org/10.1016/S0031-9201(03)00158-4.

Assumpção, M., Bianchi, M., Julià, J., Dias, F.L., França, G.S., Nascimento, R., Drouet, S., Pavão, C.G., Albuquerque, D.F., Lopes, A.E.V., 2013. Crustal thickness map of Brazil: data compilation and main features. J. S. Am. Earth Sci. 43, 74–85. http://dx.doi.org/10.1016/j.jsames.2012.12.009.

Biggin, A., van Hinsbergen, D.J.J., Langereis, C.G., Straathof, G.B., Deenen, M.H., 2008. Geomagnetic secular variation in the Cretaceous Normal Superchron and in the Jurassic. Phys. Earth Planet. Inter. 169, 3–19. http://dx.doi.org/10.1016/j.pepi.2008.07.004.

Braitenberg, C., 2015. Exploration of tectonic structures with GOCE in Africa and across-continents. Int. J. Appl. Earth Obs. Geoinf. 35 (A), 88–95. http://dx.doi.org/10.1016/j.jag.2014.01.013.

Buiter, S.J.H., Torsvik, T.H., 2014. A review of Wilson Cycle plate margins: a role for mantle plumes in continental break-up along sutures? Gondwana Res. 26, 627–653. http://dx.doi.org/10.1016/j.gr.2014.02.007.

Butler, R.F., 1992. Paleomagnetism: Paleomagnetism: Magnetic Domains to Geologic Terranes. Blackwell Scientific Publications Boston.

Casquet, C., Rapela, C.W., Pankhurst, R.J., Baldo, E.G., Galindo, C., Fanning, C.M., Dahlquist, J.A., Saavedra, J., 2012. A history of Proterozoic terranes in southern South America: from Rodinia to Gondwana. Geosci. Front. 3 (2), 137–145.

Chulick, G.S., Detweiler, S., Mooney, W.D., 2013. Seismic structure of the crust and uppermost mantle of South America and surrounding oceanic basins. J. S. Am. Earth Sci. 42, 260–276. http://dx.doi.org/10.1016/j.jsames.2012.06.002.

Collier, J.S., McDermott, C., Warner, G., Gyori, N., Schnabel, M., McDermott, K., Horn, B.W., 2017. New constraints on the age and style of continental breakup in the South Atlantic from magnetic anomaly data. Earth Planet. Sci. Lett. 477, 27–40. http://dx.doi.org/10.1016/j.epsl.2017.08.007.

Deenen, M.H.L., Langereis, C.G., van Hinsbergen, D.J.J., Biggin, A.J., 2011. Geomagnetic secular variation and the statistics of palaeomagnetic directions. Geophys. J. Int. 186, 509–520. http://dx.doi.org/10.1111/j.1365-246X.2011.05050.x.

Dirks, P.H.G.M., Blenkinsop, T.G., Jelsma, H.A., 2009. The geological evolution of Africa. In: De Vito, B., Grasemann, B., Stuwe, K. (Eds.), Geology. Encyclopedia of Life Support Systems (EOLSS) IV. Eolss Publishers, Paris, France, 978-1-84826-457-1, pp. 230–251.

Dodd, S.C., MacNiocaill, C., Muxworthy, A.R., 2015. Long duration (> 4 Ma) and steady-state volcanic activity in the early Cretaceous Paraná–Etendeka Large Igneous Province: new palaeomagnetic data from Namibia. Earth Planet. Sci. Lett. 414, 16–29. http://dx.doi.org/10.1016/j.epsl.2015.01.009.

Dunlop, D., Özdemir, O., 1997. Rock Magnetism: Fundamentals and Frontiers. Cambridge University Press London, London.

Ernesto, M., Pacca, I.G., Hyodo, F.Y., Nardy, A.J.R., 1990. Paleomagnetism of the Mesozoic Serra Geral formation, southern Brazil. Phys. Earth Planet. Inter. 64, 153–175.

Ernesto, M., Comin-Chiaramonti, P., Gomes, C.B., Piccirillo, E.M., Castillo, A.M., Velázquez, J.C., 1996. Paleomagnetic data from the Central Alkaline Province, Eastern Paraguay. In: Gomes, C.B., Comin-Chiaramonti, P. (Eds.), Alkaline Magmatism in Central-Eastern Paraguay. USPFAPESP, pp. 85–102.

Ernesto, M., Raposo, M.I., Marques, L.S., Renne, P.R., Diogo, L.A., de Min, A., 1999. Paleomagnetism, geochemistry and $^{40}Ar/^{39}Ar$ dating of the North-eastern Paraná Magmatic Province: tectonic implications. J. Geodyn. 28, 321–340.

Ewart, A., Marsh, J.S., Milner, S.C., Duncan, A.R., Kamber, B.S., Armstrong, R.A., 2004a. Petrology and geochemistry of Early Cretaceous bimodal continental flood volcanism of the NW Etendeka, Namibia. Part 1: introduction, mafic lavas and re-evaluation of mantle source components. J. Petrol. 45 (1), 59–105. http://dx.doi.org/10.1093/petrology/egg083.

Ewart, A., Marsh, J.S., Milner, S.C., Duncan, A.R., Kamber, B.S., Armstrong, R.A., 2004b. Petrology and geochemistry of Early Cretaceous bimodal continental flood volcanism of the NW Etendeka, Namibia. Part 2: characteristics and petrogenesis of the high-Ti latite and high-Ti and low-Ti voluminous quartz latite eruptives. J. Petrol. 45 (1), 107–138. http://dx.doi.org/10.1093/petrology/egg082.

Fisher, R., 1953. Dispersion on a sphere. Proceedings of the Royal Society of London. Series A, Mathematical and Physical Sciences 217, 295–305.

Frindt, S., Trumbull, R.B., Romer, L.R., 2004. Petrogenesis of the Gross Spitzkoppe topaz granite, central western Namibia: a geochemical and Nd–Sr–Pb isotope study. Chem. Geol. 206, 43–71. http://dx.doi.org/10.1016/j.chemgeo.2004.01.015.

Gaina, C., Torsvik, T.H., van Hinsbergen, D.J.J., Medvedev, S., Werner, S.C., Labails, C., 2013. The African Plate: a history of oceanic crust accretion and subduction since the Jurassic. Tectonophysics 604, 4–25. http://dx.doi.org/10.1016/j.tecto.2013.05.037.

Gee, J., Kent, D.V., 2007. Source of oceanic magnetic anomalies and the geomagnetic polarity time scale. In: Kono, M. (Ed.), Treatise on Geophysics. Elsevier, Amsterdam, pp. 455–507.

Gidskehaug, A., Creer, K.M., Mitchell, J.G., 1975. Palaeomagnetism and K-Ar ages of the South West African basalts and their bearing on the time of initial rifting of the South Atlantic Ocean. Geophys. J. R. Astron. Soc. 42, 1–20.

Goguitchaichvili, A., Solano, M.C., Camps, P., Bettucci, L.S., Mena, M., Trindade, R., Reyes, B.A., Morales, J., Loera, H.L., 2012. The Earth's magnetic field prior to the Cretaceous Normal Superchron: new palaeomagnetic results from the Alto Paraguay Formation. Int. Geol. Rev. 1–13. http://dx.doi.org/10.1080/00206814.2012.732801.

Gradstein, F.M., Agterberg, F.P., Ogg, J.O., Hardenbol, J., van Veen, P., Thierry, J., Huang, Z., 1994. A Mesozoic time scale. J. Geophys. Res. 99, 24051–24074.

Haggerty, S.E., 1991. Oxide textures — a mini-atlas. In: Lindsley, D.H. (Ed.), Oxide Minerals: Petrologic and Magnetic Significance. Reviews in Mineralogy 25. pp. 129–219.

Heine, C., Zoethout, J., Müller, R.D., 2013. Kinematics of the South Atlantic rift. Solid Earth Discuss. 5, 41–116. http://dx.doi.org/10.5194/se-4-215-2013.

Janasi, V.A., de Freitas, V.A., Heaman, L.H., 2011. The onset of flood basalt volcanism, Northern Paraná Basin, Brazil: a precise U–Pb baddeleyite/zircon age for a Chapecó-type dacite. Earth Planet. Sci. Lett. 302, 147–153. http://dx.doi.org/10.1016/j.epsl.2010.12.005.

Kent, J.T., Briden, J.C., Mardia, K.V., 1983. Linear and planar structure in ordered multivariate data as applied to progressive demagnetisation of palaeomagnetic remanence. Geophys. J. R. Astron. Soc. 81, 75–87.

Kirstein, L.A., Kelley, S., Hawkesworth, C., Turner, S., Mantovani, M., Wijbrans, J., 2001. Protracted felsic magmatic activity associated with the opening of the South Atlantic. J. Geol. Soc. Lond. 158, 583–592.

Koopmann, H., Schreckenberger, B., Franke, D., Becker, K., Schnabel, M., 2014. The late rifting phase and continental break-up of the southern South Atlantic: the mode and timing of volcanic rifting and formation of earliest oceanic crust. In: Wright, T.J., Ayele, A., Ferguson, D.J., Kidane, T., Vye-Brown, C. (Eds.), Magmatic Rifting and Active Volcanism. 420 Geological Society Special Publication, London. http://dx.doi.org/10.1144/SP420.2.

Koymans, M.R., Langereis, C.G., Pastor-Galan, D., van Hinsbergen, D.J.J., 2016. Paleomagnetism.org: an online multi-platform open source environment for paleomagnetic data analysis. Comput. Geosci. 93, 127–137. http://dx.doi.org/10.1016/j.cageo.2016.05.007.

Lustrino, M., Melluso, L., Brotzu, P., Gomes, C.B., Morbidelli, L., Muzio, R., Ruberti, E.,

Tassinari, C.C.G., 2005. Petrogenesis of the Early Cretaceous Valle Chico Igneous Complex (SE Uruguay): relationships with Paraná–Etendeka magmatism. Lithos 82, 407–434. http://dx.doi.org/10.1016/j.lithos.2004.07.004.

Luttinen, A.V., Heinonen, J.S., Kurhila, M., Jourdan, F., Mänttäri, I., Vuori, S.K., Huhma, H., 2015. Depleted mantle-sourced CFB magmatism in the Jurassic Africa-Antarctia rift: petrology and $^{40}Ar/^{39}Ar$ and U/Pb chronology of the Vestfjella dyke swarm, Dronning Maud Land, Antarctica. J. Petrol. 56 (5), 919–952. http://dx.doi.org/10.1096/petrology/egv022.

Manton, W.I., Siedner, G., 1967. Age of the Paresis complex, South-West Africa. Nature 216, 1197–1198.

Marsh, J.S., Ewart, A., Milner, S.C., Duncan, A.R., 2001. The Etendeka Igneous Province: magma types and their stratigraphic distribution with implications for the evolution of the Paraná-Etendeka flood basalt province. Bull. Volcanol. 62, 464–486. http://dx.doi.org/10.1007/s004450000115.

Marzoli, A., Melluso, L., Morra, V., Renne, P.R., Sgrosso, I., D'Antonio, M., Duarte Morais, L., Morais, E.A.A., Ricci, G., 1999. Geochronology and petrology of Cretaceous basaltic magmatism in the Kwanza basin (Angola) and relationships with the Paraná-Etendeka continental flood basalt province. J. Geodyn. 8, 341–356.

Maus, S., Sazonova, T., Hemant, K., Fairhead, J.D., Ravat, D., 2007. National geophysical data center candidate for the World Digital Magnetic Anomaly Map. Geochem. Geophys. Geosyst. 8 (6), Q06017. http://dx.doi.org/10.1029/2007GC001643.

McFadden, P.L., McElhinny, M.W., 1988. The combined analysis of remagnetization circles and direct observations in palaeomagnetism. Earth Planet. Sci. Lett. 87, 161–172.

McFadden, P., McElhinny, M., 1990. Classification of the reversal test in palaeomagnetism. J. Geophys. Res. 96, 3923–3933.

McNeill, G.W., 1989. A Geochemical Study of Three Namibian Igneous Complexes. MSc Thesis,. University of St. Andrews.

Mena, M., Orgeira, M.J., Lagorio, S.L., 2006. Paleomagnetism, rock-magnetism and geochemical aspects of early Cretaceous basalts of the Paraná Magmatic Province, Misiones, Argentina. Earth, Planets and Space 58, 1283–1293.

Miller, R.M., 2008. Early Cretaceous Etendeka Group. In: Miller, R.M. (Ed.), The Geology of Namibia Vol. 3: Palaeozoic to Cenozoic. Windhoek: Geological Survey of Namibia Windhoekpp. 17-1–17-57.

Milner, S.C., Duncan, A.R., Ewart, A., 1992. Quartz latite rheoignimbrite flows of the Etendeka Formation, north-western Namibia. Bull. Volcanol. 54, 200–219.

Milner, S.C., Le Roex, A.P., Watkins, R.T., 1993. Rb–Sr age determination of rocks from the Okenyenya igneous complex, northwestern Namibia. Geol. Mag. 130, 335–343.

Milner, S.C., Duncan, A.R., Whittingham, A.M., Ewart, A., 1995a. Trans-Atlantic correlation of eruptive sequences and individual silicic volcanic units within the Pararaná-Etendeka igneous province. J. Volcanol. Geotherm. Res. 69, 137–157.

Milner, S.C., Le Roex, A.P., O'Connor, J.M., 1995b. Age of Mesozoic igneous rocks in northwestern Namibia, and their relationship to continental breakup. J. Geol. Soc. Lond. 152, 97–104. http://dx.doi.org/10.1144/gsjgs.152.1.0097.

Moskowitz, B.M., 1981. Methods for estimating Curie temperatures of titanomaghemites from experimental JS-T data. Earth Planet. Sci. Lett. 53, 84–88.

Moulin, M., Aslanian, D., Unternher, P., 2010. A new starting point for the South and Equatorial Atlantic Ocean. Earth Sci. Rev. 98, 1–37. http://dx.doi.org/10.1016/j.earscirev.2009.08.001.

Nürnberg, D., Müller, R.D., 1991. The tectonic evolution of the South Atlantic from late Jurassic to present. Tectonophysics 191, 27–53. http://dx.doi.org/10.1016/0040-1951(91)90231-G.

Owen-Smith, T.M., Ashwal, L.D., Sudo, M., Trumbull, R.B., 2017. Age and petrogenesis of the Doros Complex, Namibia, and implications for early plume-derived melts in the Paraná–Etendeka LIP. J. Petrol. 58 (3), 423–442. http://dx.doi.org/10.1093/petrology/egx021.

Peate, D.W., 1997. Parana-Etendeka Province. In: Mahoney, J.J., Coffin, M.F. (Eds.), Large Igneous Provinces: Continental, Oceanic and Planetary Flood Volcanism. Geophysical Monograph 100. pp. 217–245.

Peate, D.W., Hawkesworth, C.J., Mantovani, S.M., 1992. Chemical stratigraphy of the Paraná lavas (South America): classification of magma types and their spatial distribution. Bull. Volcanol. 55, 119–139.

Pérez-Díaz, L., Eagles, G., 2014. Constraining South Atlantic growth with seafloor spreading data. Tectonics 33. http://dx.doi.org/10.1002/(ISSN)1944-9194.2014TC003644.

Pinto, V.M., Hartmann, L.A., Santos, J.O., McNaughton, N.J., Wildner, W., 2011. Zircon U–Pb geochronology from the Paraná bimodal volcanic province support a brief eruptive cycle at ~135 Ma. Chem. Geol. 281, 93–102. http://dx.doi.org/10.1016/j.chemgeo.2010.11.031.

Pirajno, F., Phillips, D., Armstrong, R.A., 2000. Volcanology and eruptive histories of the Erongo volcanic complex and the Paresis igneous complex, Namibia: implications for mineral deposit styles. Communications of the Geological Survey of Namibia 12, 301–312.

Polteau, S., Hendriks, B.W.H., Planke, S., Ganerød, M., Corfu, F., Faleide, J.I., Midtkandal, I., Svensen, H., Myklebust, R., 2016. The Early Cretaceous Barents Sea Sill Complex: distribution, $^{40}Ar/^{39}Ar$ geochronology, and implications for carbon gas formation. Palaeogeogr. Palaeoclimatol. Palaeoecol. 441, 83–95. http://dx.doi.org/10.1016/j.palaeo.2015.07.007.

Raposo, M.I., Ernesto, M., 1995. An Early Cretaceous paleomagnetic pole from Ponta Grossa dikes (Brazil): implications for the South American Mesozoic apparent polar wander path. J. Geophys. Res. 100 (B10), 20095–20109.

Renne, P.R., Ernesto, M., Pacca, I.G., Coe, R.S., Glen, J.M., Prévot, M., Perrin, M., 1992. The age of Paraná flood volcanism, rifting of Gondwanaland, and the Jurassic-Cretaceous boundary. Science 258, 137–157.

Renne, P.R., Glen, J.M., Milner, S.C., Duncan, A.R., 1996. Age of Etendeka flood volcanism and associated intrusions in southwestern Africa. Geology 24 (7), 659–662. http://dx.doi.org/10.1130/0091-7613(1996)024<0659:AOEFVA>2.3.CO;2.

Renne, P.R., Mundil, R., Balco, G., Min, K., Ludwig, K.R., 2010. Joint determination of ^{40}K decay constants and $^{40}Ar/^{40}K$ for the Fish Canyon sanidine standard, and improved accuracy for $^{40}Ar/^{39}Ar$ geochronology. Geochim. Cosmochim. Acta 4, 5349–5367. http://dx.doi.org/10.1016/j.gca.2010.06.017.

Schmitt, A.K., Emmermann, R., Trumbull, R., Bühn, B., Henjes-Kunst, F., 2000. Petrogenesis and $^{40}Ar/^{39}Ar$ geochronology of the Brandberg Complex, Namibia: evidence for a major mantle contribution in metaluminous and peralkaline granites. J. Petrol. 41, 1207–1239.

Seton, M., Whittaker, J.M., Wessel, P., Müller, R.D., DeMets, C., Merkouriev, S., Cande, S., Stock, J., Gaina, C., Eagles, G., Granot, R., Wright, N., Williams, S.E., 2014. Community infrastructure and repository for marine magnetic identifications. Geochemistry, Geophysics, Geosystems Technical Brief 15 (4), 1629–1641. http://dx.doi.org/10.1002/2013GC005176.

Solano, M., Goguitchaichvili, A., Sánchez Bettucci, L., Ruiz, R., Calvo-Rathert, M., Ruiz-Martinez, V., Soto, R., Alva-Valdivia, L., 2010. Paleomagnetism of Early Cretaceous Arapey Formation (Northern Uruguay). Stud. Geophys. Geod. 54 (4), 533–546. http://dx.doi.org/10.1007/s11200-010-0032-8.

Stewart, K., Turner, S., Kelley, S., Hawkesworth, C., Kirstein, L., Mantovani, M., 1996. 3-D, ^{40}Ar-^{39}Ar geochronology in the Paraná continental flood basalt province. Earth Planet. Sci. Lett. 143, 95–109.

Tamrat, E., Ernesto, M., 1999. Magnetic fabric and rock-magnetic character of the Mesozoic flood basalts of the Paraná Basin, Brazil. J. Geodyn. 28, 419–437.

Thiede, D.S., Vasconcelos, P.M., 2010. Paraná flood basalts: rapid extrusion hypothesis confirmed by new $^{40}Ar/^{39}Ar$ results. Geology 38, 747–750.

Torsvik, T.H., Cocks, L.R.M., 2017. Earth History and Palaeogeography. Cambridge University Press, pp. 317.

Torsvik, T.H., Briden, J.C., Smethurst, M.A., 2000. Super-IAPD Interactive Analysis of Palaeomagnetic Data. www.geodynamics.no/software.htm.

Torsvik, T.H., Rousse, S., Labails, C., Smethurst, M.A., 2009. A new scheme for the opening of the South Atlantic Ocean and the dissection of an Aptian salt basin. Geophys. J. Int. 177 (3), 1315–1333. http://dx.doi.org/10.1111/j.1365-246X.2009.04137.x.

Torsvik, T.H., Van der Voo, R., Preeden, U., Mac Niocaill, C., Steinberger, B., Doubrovine, P.V., van Hinsbergen, D.J.J., Domeier, M., Gaina, C., Tohver, E., Meert, J.G., McCausland, P.J.A., Cocks, L.R.M., 2012. Phanerozoic polar wander, palaeogeography and dynamics. Earth Sci. Rev. 114, 325–368. http://dx.doi.org/10.1016/j.earscirev.2012.06.007.

Turner, S., Regelous, M., Kelley, S., Hawkesworth, C., Mantovani, M., 1994. Magmatism and continental break-up in the South Atlantic: high precision $^{40}Ar/^{39}Ar$ geochronology. Earth Planet. Sci. Lett. 121, 333–348.

Unternehr, P., Curie, D., Olivet, J.L., Goslin, J., Beuzart, P., 1988. South Atlantic fits and intraplate boundaries in Africa and South America. Tectonophysics 155, 169–179. http://dx.doi.org/10.1016/0040-1951(88)90264-8.

Vandamme, D., 1994. A new method to determine paleosecular variation. Phys. Earth Planet. Inter. 85, 131–142.

Verati, C., Jourdan, F., 2014. Modelling effect of sericitization of plagioclase on the $^{40}K/^{40}Ar$ and $^{40}Ar/^{39}Ar$ chronometers: implication for dating basaltic rocks and mineral deposits. Geol. Soc. Spec. Publ. 378, 155–174. http://dx.doi.org/10.1144/SP378.14.

Verwoerd, W.J., Retief, E.A., Prins, P., 2000. The Etanenoberg alkaline complex, Namibia. Communications of the Geological Survey of Namibia 12, 291–300.

Wigand, M., Schmitt, A.K., Trumbull, R.B., Villa, I.M., Emmermann, R., 2004. Short-lived magmatic activity in an anorogenic subvolcanic complex: $^{40}Ar/^{39}Ar$ and ion microprobe U-Pb zircon dating of the Erongo, Damaraland, Namibia. J. Volcanol. Geotherm. Res. 130, 285–305. http://dx.doi.org/10.1016/S0377-0273(03)00310-X.

Wilkinson, C.M., Ganerød, M., Hendriks, B.W.H., Eide, E.A., 2016. Compilation and appraisal of geochronological data from the North Atlantic Igneous Province (NAIP). In: Peron-Pinvidic, G., Hopper, J.R., Stoker, M.S., Gaina, C., Doornenbal, J.C., Funck, T., Arting, U.E. (Eds.), The NE Atlantic Region: A Reappraisal of Crustal Structure, Tectonostratigraphy and Magmatic Evolution. Geological Society, London, Special Publicationspp. 447. http://dx.doi.org/10.1144/SP447.10.